Journal of Applied Mechanics and Technical Physics, Vol. 45, No. 6, pp. 860–870, 2004

SOLVING THE PROBLEM OF GRAVITATIONAL COMPRESSION OF A LAYERED SPHERE (BY THE EXAMPLE OF THE EARTH)

L. V. Baev and V. N. Solodovnikov

UDC 539.3

The problem of spherically symmetric, gravitational compression of an isotropic hyperelastic layered sphere which modeling the region of the Earth below the Mohorovičič boundary is solved. The known mechanical characteristics of the Earth in the compressed state are used to find its characteristics in the unstrained state obtained by adiabatic or isothermal stress relief. The stress state differs significantly from the state of purely hydrostatic compression. The minimum bulk compression and maximum radial tension occur not on the boundary of the sphere but in depth at certain distances from the boundary.

Key words: *the Earth, adiabatic or isothermal stress relief, isotropic hyperelasticity, mechanical characteristics.*

1. Elastic Characteristics of the Earth. We consider a sphere of radius $\hat{R}_1 = 6341$ km which models a region of the Earth (the Earth radius is $\hat{R} = 6371$ km; the upper boundary of the region is at a depth $\hat{R} - \hat{R}_1 = 30$ km). In the solution proposed, this region is partitioned into five layers which correspond to the layers adopted in geophysics: layers B, C, and D in the mantle, the outer core E, and the inner core G with discontinuities introduced for the functions defining the state of the material or their derivatives at the boundary points between the layers. Layer F, which is intermediate between layers G and E, is also replaced by a discontinuity surface. The partitioning is performed using the data of [1].

According to the distributions of the density $\hat{\rho}$ and the propagation velocities of longitudinal and transverse waves v_p and v_s at points (nodes) along the radius of the compressed Earth $\hat{r}$ given in [1], we choose boundary points between layers A, B, C, D, E, and G with radial coordinates $\hat{r}_A = \hat{R}_1 = 6341$, $\hat{r}_B = 5971$, $\hat{r}_C = 5371$, $\hat{r}_D = 3482$, $\hat{r}_E = 1211$ (km) [A is the layer above the surface $\hat{r} = \hat{R}_1$; Bullen [1] gives the depths rather than radial coordinates of the nodal points $(\hat{R} - \hat{r})$; in the present paper, the depths of the boundary points take values of 30, 400, 1000, 2889, and 5160 km, respectively]. At the boundary points, the values of $\hat{\rho}$, v_p, and v_s [1] are assumed to refer to the underlying layer unless they are considered continuous. For discontinuous $\hat{\rho}$, v_p, and v_s, the values at the boundary point that refer to the overlying layer are found by extrapolation of their values at the nodes of this layer. Continuous quantities are v_p at the point $\hat{r}_B$, $\hat{\rho}$ at the point $\hat{r}_E$, and $\hat{\rho}$, v_p, and v_s at the point $\hat{r}_C$ but it is assumed that the derivatives of these functions may be discontinuous. With introduction of discontinuities, none of the values of $\hat{\rho}$, v_p, and v_s given in [1] is corrected. At the boundary points $\hat{r}_B$, $\hat{r}_D$, and $\hat{r}_E$, limiting values are added which refer to the overlying layer. After extrapolation, the nodes at 3485 km and 1251 km are not used as they are too close to the points $\hat{r}_D$ and $\hat{r}_E$.

The values of $\hat{\rho}$, v_p, and v_s are used to calculate the shear and bulk moduli of the material in the compressed state of the Earth [1]:

$$\mu = \hat{\rho} v_s^2, \qquad K = \hat{\rho}(v_p^2 - 4v_s^2/3).$$

Lavrent'ev Institute of Hydrodynamics, Siberian Division, Russian Academy of Sciences, Novosibirsk 630090; volk@hydro.nsc.ru. Translated from Prikladnaya Mekhanika i Tekhnicheskaya Fizika, Vol. 45, No. 6, pp. 103–115, November–December, 2004. Original article submitted November 3, 2003; revision submitted February 10, 2004.

TABLE 1

Characteristic of the Earth in Compressed and Unloaded States

Node	$\hat{r}$, km	$\hat{r}'$	$\hat{\rho}$, g/cm^3	v_p, km/sec	v_s, km/sec	K, 10^5 MPa	μ, 10^5 MPa	ν	ρ, g/cm^3	K_0, 10^5 MPa	μ_0, 10^5 MPa	ν_0
1	6341	1	3.32	7.74	4.62	1.044	0.7086	0.2233	2.909	0.6335	0.6209	0.1306
2	6271	0.989	3.35	7.95	4.5	1.213	0.6784	0.2643	2.933	0.7341	0.594	0.1814
3	6171	0.9732	3.39	8.26	4.5	1.398	0.6865	0.289	2.945	0.8222	0.5963	0.208
4	6071	0.9574	3.42	8.59	4.5	1.6	0.6926	0.3109	2.953	0.9207	0.5979	0.2331
5	5971	0.9417	3.44	8.92	4.5	1.808	0.6966	0.3293	2.954	1.021	0.5982	0.2549
	5971	0.9417	3.77	8.92	4.72	1.88	0.8399	0.3056	3.222	1.044	0.7179	0.2203
6	5721	0.9022	4.17	10.48	5.8	2.71	1.403	0.2792	3.489	1.396	1.174	0.1717
7	5371	0.8471	4.54	11.44	6.36	3.493	1.836	0.2763	3.714	1.664	1.502	0.1531
8	4371	0.6893	5.09	12.79	6.92	5.077	2.437	0.2931	3.941	2.007	1.887	0.1421
9	3671	0.5789	5.4	13.61	7.26	6.208	2.846	0.3011	4.05	2.209	2.135	0.1345
10	3482	0.5491	5.695	13.64	7.3	6.549	3.036	0.2993	4.234	2.264	2.257	0.1259
	3482	0.5491	9.95	8.12	0	6.561	0.05	0.4962	7.813	2.72	0.0393	0.4928
11	2371	0.3739	11.39	9.53	0	10.34	0.05	0.4976	7.879	2.834	0.0346	0.4939
12	1211	0.191	12.74	10.347	0	13.64	0.05	0.4982	8.578	3.43	0.0337	0.4951
	1211	0.191	12.74	11.25	3.86	13.59	1.898	0.4333	8.557	3.393	1.275	0.333
13	0	0	13.03	11.25	2.91	15.02	1.103	0.4641	8.715	3.699	0.7379	0.4065

In the outer core (at $v_s = 0$), the zero value for μ is replaced by $\mu = 5 \cdot 10^3$ MPa, which is much smaller than that in the remaining layers. The coordinates of the nodes $\hat{r}$, the values of $\hat{r}' = \hat{r}/\hat{R}_1$, $\hat{\rho}$, v_p, v_s, K, and μ, and Poisson's constant $\nu = (3K - 2\mu)/[2(3K + \mu)]$ at the nodes are given in Table 1. Nodes 1, 2, 3, 4, and 5 are in layer B, nodes 5, 6, and 7 in layer C; nodes 7, 8, 9, and 10 layer D; nodes 10, 11, and 12 in the outer core; and nodes 12 and 13 in the inner core. Nodes 1, 5, 7, 10, and 12 are the boundary points between the layers with the coordinates $\hat{r}_A$, $\hat{r}_B$, $\hat{r}_C$, $\hat{r}_D$, and $\hat{r}_E$, respectively; node 13 is at the center $\hat{r} = 0$. Tables 1 and 2 give a pair of values for each of the parameters at nodes 5, 10, and 12; the first value refers to the overlying layer and the second value to the underlying layer; for continuous parameters, two identical values are given; at node 7, the parameters are continuous.

Thus, instead of regions of fast changes of $\hat{\rho}$, v_p, v_s, K, μ, and ν given in [1], the above five-layer partitioning allows one to introduce discontinuity surfaces of these parameters and to obtain smoother distributions of these parameters and the sought functions obtained using them in each layer. The data of [1] are also discussed in [2–4].

2. Constitutive Equations. We assume that after removal of gravitational forces in the entire region, the material considered isotropic hyperelastic [5] can pass (in an adiabatic or an isothermally reversible manner) to a state with zero stresses and strains without failure and loss of continuity. This implies continuity of the radial coordinates of material points in the unloaded and compressed state $r \geqslant 0$, $\hat{r} \geqslant 0$, one-to-one correspondence between them $\hat{r} = \hat{r}(r)$, and satisfaction of the inequality $\hat{r}_{,r} > 0$. The proposition of the theory of isotropic hyperelastic bodies on coaxiality of the stress and strain tensors in this problem is valid by virtue of spherical symmetry.

We introduce the strain tensor invariants

$$J = (\varepsilon_m \varepsilon_n \varepsilon_l)^{1/2}, \qquad \Upsilon = \frac{\varepsilon_m^2 + \varepsilon_n^2 + \varepsilon_l^2}{(\varepsilon_m + \varepsilon_n + \varepsilon_l)^2} - \frac{1}{3}, \qquad I_1 = \frac{1}{2}(\varepsilon_m + \varepsilon_n + \varepsilon_l) \tag{2.1}$$

(m, n, l is an even permutation of subscripts 1, 2, and 3).

Here and below, ε_i are the squares of the main multiplicities of the elongations, i.e., the ratios of the current to the initial values of the squared length of the elementary material fibers passing along the principal axes of the strain tensors; they are related to the main components of the Green strain tensor e_i by the equalities $\varepsilon_i = 1 + 2e_i$ (for zero fiber strain, $\varepsilon_i = 1$; in the case of fiber elongation, $\varepsilon_i > 1$ and increases; and in the case of fiber shortening, $\varepsilon_i < 1$ and decreases); J is the ratio of the current to the initial value of the elementary volume or the Jacobian

of transformation of the initial Cartesian coordinates of the material points to the current coordinates [the bulk strain equal to $(J-1)$ is compression for $J<1$ and tension for $J>1$]; in space with Cartesian coordinates ε_i, the value of $\Upsilon = I_2 I_1^{-2}$ equals one-third of the squared slope of the radius vector of the given point to the half-line $\varepsilon_1=\varepsilon_2=\varepsilon_3$; I_2 is the shear strain intensity. The inequalities $\varepsilon_i>0$, $I_1>0$, $0\leqslant\Upsilon<2/3$, and $J>0$ hold. The subscript i takes values $1, 2$, and 3; the variable in the subscript after the comma denotes partial differentiation.

In isotropic hyperelastic bodies, the main components of the Cauchy stress tensor (physical components of stresses) are found from the constitutive equations [6, 7]

$$\hat\sigma_i = \hat\mu\varepsilon_i(\varepsilon_i-\hat\chi)+p, \tag{2.2}$$

where $\hat\mu=\beta I_1^{-2}J^{-1}$, $\hat\chi=2I_1(\Upsilon+1/3)$, $\beta=\Psi_{,\Upsilon}$, $p=\Psi_{,J}=(\hat\sigma_m+\hat\sigma_n+\hat\sigma_l)/3$ is the average pressure (compression pressure for $p<0$ and extension pressure for $p>0$), and Ψ is the strain energy density, a determining function specified for materials. In spherically symmetric states, the stresses and strains in all directions orthogonal to the radial direction are identical: $\hat\sigma_2=\hat\sigma_3$, $\varepsilon_2=\varepsilon_3=(\hat r/r)^2$ and in the radial direction, $\varepsilon_1=(\hat r_{,r})^2$.

In adiabatic processes, Ψ is determined from the increment in the internal energy density as a function of Υ, J, and S at a constant entropy density per unit volume of the unstrained body S; in isothermal processes, it is determined from the increment in the free-energy density as a function of Υ, J, and T at constant absolute temperature T. The values of the argument S in adiabatic processes and the values of the argument T in isothermal processes can be different at different points but at each material point, they remain constant. Therefore, Ψ depends on only two arguments Υ and J. The shear and bulk moduli μ_0 and K_0 appearing in the expression for Ψ and describing the material in the unstrained state are found from the solution the problem using the known characteristics of the material in the strained state.

The relationship between the pressure and bulk strain is described by the Birch–Murnaghan equation [8, 9]

$$p=(3/2)K_0(J^{-5/3}-J^{-7/3}), \tag{2.3}$$

where K_0 is the bulk modulus of the material in the initial unstrained state ($p_{,J}=K_0$ at $J=1$). As the volume decreases, the pressure p increases in absolute value.

The assumption that p depends only on J implies that the derivatives $p_{,\Upsilon}=\beta_{,J}=0$ and hence, β depends only on one argument Υ. Because of lack of data on the dependence of β on Υ and because of insignificant changes in Υ, we assume, as a first approximation, that β is a constant with the same value as in Hooke's law: $\beta=9\mu_0/4$. As a result, Ψ is represented as the sum of two terms — the shear and bulk strain energy densities, each of which depends only on one argument:

$$\Psi=\Psi_1+\Psi_2,\qquad \Psi_1=(9\mu_0/4)\Upsilon,\qquad \Psi_2=(9K_0/8)(1-J^{-2/3})^2.$$

As the strains tend to zero, Ψ continuously becomes a determining function of Hooke's law with the same two material constants as in Hooke's law: $\mu_0=E_0/[2(1+\nu_0)]$ and $K_0=E_0/[3(1-2\nu_0)]$ (E_0 and ν_0 are the Young's modulus and Poisson's constant for the unstrained material, respectively).

We note that at large strains, the condition of constancy or even boundedness of β implies the existence of dropping stress–strain curves.

3. Relationship of Elastic Characteristics of the Material in the Strained and Unstrained States. In [1], the stress and strain increments due to propagation of longitudinal and transverse waves are related by a linear Hooke's law for an isotropic material with two constants — shear and bulk moduli μ and K. For the components of the Yauman stress rate tensor $\hat\Sigma$ and the strain rate tensor $\hat\eta$ that generate these increments, the Hooke's law is written as follows (m, n, l is an even permutation of subscripts 1, 2, and 3):

$$\hat\Sigma_{mm}=2\mu\hat\eta_{mm}+(K-2\mu/3)(\hat\eta_{mm}+\hat\eta_{nn}+\hat\eta_{ll}),\qquad \hat\Sigma_{mn}=2\mu\hat\eta_{mn}. \tag{3.1}$$

Let us find the relationship of μ and K with the shear and bulk moduli μ_0 and K_0 of the unstrained material according to the theory of isotropic hyperelastic bodies [5–7].

We assume that the pressure increment Δp is proportional to the bulk strain increment determined with respect to the current volume of the material with the coefficient — a bulk modulus K: $\Delta p=KJ^{-1}\Delta J$. Letting the increment of the Jacobian ΔJ tend to zero, we arrive at the equality $p_{,J}=KJ^{-1}$, which coincides with that given in [1] (taking into account the opposite sign of p in [1] and the expression of $J=\rho/\hat\rho$ in terms of the initial and current density ρ and $\hat\rho$). From this and from (2.3), we obtain the relation linking the bulk moduli in the unloaded

and compressed states: $K = (1/2)K_0(7J^{-7/3} - 5J^{-5/3})$. As the volume decreases, the resistance to the additional deformation increases: $K \to \infty$ at $J \to 0$.

Let us find the relationship between μ and μ_0. In isotropic hyperelastic bodies, the nondiagonal components of the tensors $\hat{\Sigma}$ and $\hat{\eta}$ [which, in this case, can have values different from those in (3.1)] satisfy the equalities [6, 7]

$$\hat{\Sigma}_{mn} = B_l\,\hat{\eta}_{mn}, \qquad B_l = \frac{9\mu_0(\varepsilon_m + \varepsilon_n)}{J(\varepsilon_m + \varepsilon_n + \varepsilon_l)^3}\,[2\varepsilon_m\varepsilon_n + (\varepsilon_m + \varepsilon_n)\varepsilon_l - \varepsilon_l^2]$$

with the coefficients B_l dependent on the current strained state of the material. We take into account that $\varepsilon_2 = \varepsilon_3$ and $B_2 = B_3$ and introduce the parameter $\xi = (\varepsilon_2 - \varepsilon_1)/(\varepsilon_2 + \varepsilon_1)$. Calculations show that the parameter ξ should be small. In this case, the coefficients $B_l > 0$ and their average value $(B_1 + 2B_2)/3$ is close to the doubled value of $\mu = \mu_0 J^{-1}$, which can be considered the shear modulus of the material in the compressed state. The relative values of the differences between B_1, B_2, and 2μ are small. They reach maxima (to 20%) near the boundary surface $\hat{r} = \hat{R}_1$ and decrease when approaching the outer core. In passing from the mantle to the outer core, the relative values of the differences increase suddenly but because μ is small in the outer core, this increase is insignificant and the differences can be ignored. In the inner core, the differences are negligible.

In the equations of isotropic hyperelastic bodies [6, 7], unlike in Eqs. (3.1), the stress rates $\hat{\Sigma}_{mm}$ are expressed in terms of the strain rates $\hat{\eta}_{ii}$ $(i = 1, 2, 3)$ with an asymmetric coefficient matrix which depends on the current strain state of the material. The differences between the components of this matrix [calculated from the results of the solution given below with satisfaction of the equalities $\mu_0 = \mu J$, $K_0 = 2K(7J^{-7/3} - 5J^{-5/3})^{-1}$] and the corresponding components of the matrix in (3.1) are considerable only in the mantle (the relative values of the differences between the diagonal components of the matrices do not exceed 3%; the relative differences between the nondiagonal components reach 40% on the boundary surface $\hat{r} = \hat{R}_1$ and decrease when approaching the outer core). In the outer and inner cores, we can ignore the differences between the components of the matrices are negligible and Eqs. (3.1) are appropriate.

Thus, setting

$$\mu_0 = \mu J, \qquad K_0 = 2K(7J^{-7/3} - 5J^{-5/3})^{-1}, \tag{3.2}$$

we arrive at the following problem: to find the coordinates of the nodes r and the values of the moduli μ_0 and K_0 of the unstrained material from the known values of μ and K at the nodes with coordinates $\hat{r}$. The coordinates r and $\hat{r}$ ($r' = r/R_1$ and $\hat{r}' = \hat{r}/\hat{R}_1$ are the nondimensional coordinates referred to the radii of the boundary surface in the unloaded and compressed state of the sphere R_1 and $\hat{R}_1$) are related via the function ε_2 by the equalities

$$r' = \hat{r}'(\varepsilon_{2(A)}/\varepsilon_2)^{1/2}, \tag{3.3}$$

where $\varepsilon_{2(A)} = (\hat{R}_1/R_1)^2$ is the value of ε_2 at the point $\hat{r}' = r' = 1$.

The values of μ_0, K_0, and r' are found by iterations. In the initial iteration for the Jacobian J, according to (2.3) and (3.2), we use the values

$$J = \Big(\frac{3K + 7p}{3K + 5p}\Big)^{3/2}$$

at a pressure $p = P$ $(P > -3K/7)$ determined form the formula of purely hydrostatic compression; setting $\varepsilon_1 = \varepsilon_2$ and $\varepsilon_2 = J^{2/3}$, we find μ_0, K_0, and r'. In the remaining iterations, J and ε_2 are taken from the solutions of equilibrium problems and μ_0, K_0, and r' are calculated by formulas (3.2) and (3.3) (in the second iteration, we use the same J as in the first iteration; new values are taken only for ε_2).

In each iteration in layers B, C, and D and in the outer core, the moduli μ_0 and K_0 are approximated as a functions of r' by interpolation polynomials passing through the nodal values and the density $\hat{\rho}$ and the mass M enclosed in a sphere of radius $\hat{r}$ are approximated by interpolation functions of the second order. We note that in layer B, to suppress the wavelike variation in μ_0 and K_0, we set the polynomials equal to the specified values of the derivatives $\mu_{0,r'}$ and $K_{0,r'}$ at the boundary point $\hat{r}_B$ and use an interpolation function of the first order for $\hat{\rho}$. In the inner core, μ_0, K_0, $\hat{\rho}$, and M are approximated by cubic polynomials with zero first- and second-order derivatives with respect to r' at the center $r' = 0$. The third-order polynomials are used to ensure the required spherical symmetry of the problem of smallness of derivatives of the sought functions with respect to r' with approach to the center. As a result, μ_0, K_0, $\hat{\rho}$, and M are found as functions r' with discontinuities of these functions or their derivative at the boundary points between the layers.

During iterations, the difference of iterations of μ_0, K_0, and r' at the nodes decrease monotonically. In the last iteration performed, the relative values of the differences between the values of μ, K, and $\hat{r}'$ given in Table 1 and calculated by the formulas $\mu = \mu_0 J^{-1}$, $K = (1/2)K_0(7J^{-7/3} - 5J^{-5/3})$, and $\hat{r}' = r'(\varepsilon_2/\varepsilon_{2(A)})^{1/2}$, increase when approaching the center $r' = 0$ but do not exceed $1.25 \cdot 10^{-4}$, $4 \cdot 10^{-4}$, and $3 \cdot 10^{-5}$, respectively, in the entire region.

4. Solution of the Problem. For spherically symmetric states, the equilibrium equation is written as

$$\hat{\sigma}_{1,\hat{r}} + \frac{2}{\hat{r}}(\hat{\sigma}_1 - \hat{\sigma}_2) + \hat{q} = 0 \qquad \Big(\hat{q} = -\frac{\gamma M \hat{\rho}}{\hat{r}^2}, \quad M = 4\pi \int\limits_0^{\hat{r}} \hat{\rho}\hat{r}^2\, d\hat{r}\Big). \tag{4.1}$$

Here $\hat{q}$ is the force of gravitational attraction from the terrestrial globe which acts per unit volume of the deformed material and points to the center of the Earth; $\gamma = 6.67 \cdot 10^{-8}$ cm^3/(g$\cdot$ sec^2) is the gravitational constant.

We integrate Eq. (4.1) over layer A to the surface $\hat{r} = \hat{R}$, where it is assumed that $\hat{\sigma}_1 = 0$. Taking into account the relatively small thicknesses of the layer and omitting the integral of the second term in (4.1), we obtain

$$\hat{\sigma}_1 = P_1 = -\int\limits_{\hat{R}_1}^{\hat{R}} \frac{\gamma M \hat{\rho}}{\hat{r}^2}\, d\hat{r} \qquad \text{at} \quad \hat{r} = \hat{R}_1, \tag{4.2}$$

which is taken to be the radial stress exerted by layer A on the underlying region of the Earth. It is estimated by the average density in layer A: $\hat{\rho} = 2.84$ g/cm^3; then $P_1 = -0.8409 \cdot 10^3$ MPa.

Integrating Eq. (4.1) from $\hat{r}$ to $\hat{R}_1$ and using (4.2), we obtain

$$\hat{\sigma}_1 = P + \int\limits_{\hat{r}}^{\hat{R}_1} \frac{2}{\hat{r}}(\hat{\sigma}_1 - \hat{\sigma}_2)\, d\hat{r}, \qquad P = -\int\limits_{\hat{r}}^{\hat{R}} \frac{\gamma M \hat{\rho}}{\hat{r}^2}\, d\hat{r} \qquad (0 \leqslant \hat{r} \leqslant \hat{R}_1), \tag{4.3}$$

where P is the pressure of purely hydrostatic compression (defined here with the sign opposite to that in [1]: $P < 0$). The stress state is not close to purely hydrostatic compression. The circumferential stresses on the surface $\hat{r} = \hat{R}_1$, as shown by the solution, are 19 times higher than the radial stresses; in almost the entire region $\hat{\sigma}_2 < \hat{\sigma}_1 < 0$, the integral on the right side of the first equality in (4.3) is positive. Therefore, P gives only the upper bound for the radial stresses $P \leqslant \hat{\sigma}_1 < 0$.

To solve the equilibrium problems, in (4.1) it is convenient to convert to the other independent variable — the initial radial coordinate r $(0 \leqslant r \leqslant R_1)$:

$$\hat{\sigma}_{1,r} + \frac{2\sqrt{\varepsilon_1}}{r\sqrt{\varepsilon_2}}(\hat{\sigma}_1 - \hat{\sigma}_2) - \frac{\gamma M \hat{\rho}\sqrt{\varepsilon_1}}{\varepsilon_2 r^2} = 0 \qquad \Big(M = 4\pi \int\limits_0^{\hat{r}} \hat{\rho}\hat{r}^2\, d\hat{r}\Big). \tag{4.4}$$

Here $\hat{\rho}$ and M are represented as functions r by interpolation of their known values at the nodes. The continuity conditions for $\hat{\sigma}_1$ and $\hat{r}$ at the boundary points between the layers and the equality $\hat{\sigma}_1 = P_1$ at $r = R_1$ are satisfied; at the center, $\hat{r} = r = 0$.

Setting $\hat{\rho} = \rho J^{-1}$ in (4.4) and considering the density in the unstrained state ρ known, we arrive at the equation

$$\hat{r}^2 \hat{\sigma}_{1,r} + (\hat{r}^2)_{,r}(\hat{\sigma}_1 - \hat{\sigma}_2) - \frac{\gamma M \rho r^2}{\hat{r}^2} = 0 \qquad \Big(M = 4\pi \int\limits_0^{r} \rho r^2\, dr\Big), \tag{4.5}$$

which, in contrast to Eqs. (4.1) and (4.4), follows, with allowance for (2.2), from the condition of stationarity of the functional

$$\Pi = \int\limits_0^{R_1} \Big(\Psi - \frac{\gamma M \rho}{\hat{r}}\Big) r^2\, dr - \frac{1}{3} P_1 \hat{R}_1^3.$$

In [7], unlike in the present study, the problem of gravitational compression of a sphere for constant ρ, μ_0, and K_0 is solved using Eqs. (4.5).

Let us calculate ε_1 and ε_2 on the surface $\hat{r} = \hat{R}_1$. Substituting the expression for the radial stress obtained from (2.1)–(2.3) for $\varepsilon_2 = \varepsilon_3$ into the equality $\hat{\sigma}_1 = P_1$, we have equation

$$\frac{9\mu_0 f}{4J} + \frac{3}{2}\,K_0(J^{-5/3} - J^{-7/3}) = P_1 \qquad \Big(f = \frac{16\xi(\xi^2-1)}{(3+\xi)^3}, \quad \xi = \frac{\varepsilon_2 - \varepsilon_1}{\varepsilon_2 + \varepsilon_1}\Big), \tag{4.6}$$

which for $\mu_0 > 0$, $K_0 > 0$, $P_1 < 0$, $-1 < \xi < 0$, $f > 0$, and $0 < J < 1$ has the unique material root J. Having determined J, we obtain

$$\varepsilon_1 = J^{2/3}\Big(\frac{1-\xi}{1+\xi}\Big)^{2/3}, \qquad \varepsilon_2 = J^{2/3}\Big(\frac{1+\xi}{1-\xi}\Big)^{1/3}. \tag{4.7}$$

The curves of p and $\hat\sigma_2$ versus ξ becomes dropping for $\xi = \xi_* = -(1+2\sqrt{7})/9 \approx -0.699$ (at this point, f takes the maximum value). Branching of the solutions of Eqs. (2.2) is ruled out if $\xi > \xi_{**} = 3 - 2\sqrt{3} \approx -0.464$ [7], which is valid in the problem considered.

Specification of the quantities μ and K on the boundary surface implies constraints on the parameter ξ. Substituting the expressions for μ_0 and K_0 from (3.2) into (4.6), we arrive at the equation

$$\frac{9\mu f}{4} + \frac{3K(J^{2/3}-1)}{7-5J^{2/3}} = P_1,$$

which is satisfied for $0 < J < 1$ only if $f < 4(3K + 7P_1)/(63\mu)$. From this it follows that $\xi > -0.363$, and this is satisfied in the problem considered.

The assumption that the shear modulus does not vary during deformation (i.e., $\mu = \mu_0$) leads to violation of the boundary conditions on the surface $\hat r = \hat R_1$. Indeed, in this case, the equation

$$\frac{9\mu f}{4J} + \frac{3K(J^{2/3}-1)}{7-5J^{2/3}} = P_1,$$

should be satisfied, which has two roots in the interval $0 < J < 1$ instead of one for $f < 0.0956$ and $\xi > -0.1424$ and does not have roots for $\xi < -0.1424$.

To solve the equilibrium problems, we use the following algorithm. We substitute into (4.4) the following expressions obtained from (2.1)–(2.3) for $\varepsilon_2 = \varepsilon_3$:

$$\hat\sigma_1 = \frac{18\mu_0\sqrt{\varepsilon_1}(\varepsilon_1-\varepsilon_2)}{(\varepsilon_1+2\varepsilon_2)^3} + \frac{3}{2}\,K_0(J^{-5/3} - J^{-7/3}), \qquad \hat\sigma_1 - \hat\sigma_2 = \frac{27\mu_0\sqrt{\varepsilon_1}(\varepsilon_1-\varepsilon_2)}{(\varepsilon_1+2\varepsilon_2)^3}.$$

Adding the equality $\varepsilon_{2,r} = (2/r)(\sqrt{\varepsilon_1\varepsilon_2} - \varepsilon_2)$ to (4.4), we arrive at the system of differential equations of the first order in ε_1 and ε_2:

$$\varepsilon_{1,r'} + \frac{1}{f_1}\Big(f_2 + \frac{f_3}{r'} - \frac{\alpha f_4}{r'^2}\Big) = 0, \qquad \varepsilon_{2,r'} - \frac{f_5}{r'} = 0 \qquad (0 \leqslant r' \leqslant 1), \tag{4.8}$$

in which

$$f_1 = \frac{9\mu_0(11\varepsilon_1\varepsilon_2 - 3\varepsilon_1^2 - 2\varepsilon_2^2)}{\sqrt{\varepsilon_1}(\varepsilon_1+2\varepsilon_2)^4} + \frac{K_0}{4\varepsilon_1}\,(7J^{-7/3} - 5J^{-5/3}), \qquad J = \varepsilon_2\sqrt{\varepsilon_1},$$

$$f_2 = \frac{18\sqrt{\varepsilon_1}(\varepsilon_1-\varepsilon_2)}{(\varepsilon_1+2\varepsilon_2)^3}\,\mu_{0,r'} + \frac{3}{2}\,(J^{-5/3} - J^{-7/3})K_{0,r'}, \qquad f_5 = 2(\sqrt{\varepsilon_1\varepsilon_2} - \varepsilon_2),$$

$$f_3 = \Big[\frac{18\mu_0\sqrt{\varepsilon_1}\,(4\varepsilon_2 - 7\varepsilon_1)}{(\varepsilon_1+2\varepsilon_2)^4} + \frac{K_0}{2\varepsilon_2}\,(7J^{-7/3} - 5J^{-5/3})\Big]f_5 + \frac{54\mu_0\varepsilon_1(\varepsilon_1-\varepsilon_2)}{\sqrt{\varepsilon_2}(\varepsilon_1+2\varepsilon_2)^3},$$

$$f_4 = \frac{M\hat\rho\sqrt{\varepsilon_1}}{\varepsilon_2}, \qquad M = 3\int\limits_0^{\hat r'} \hat\rho\hat r'^2\,d\hat r', \qquad \alpha = \alpha_1\varepsilon_{2(A)}^{1/2}, \qquad \alpha_1 = \frac{4\pi G}{3\mu_*}\,\rho_*^2\hat R_1^2;$$

α_1 and α are dimensionless constants; the expression for α includes the sought quantity $\varepsilon_2 = \varepsilon_{2(A)}$ at $r' = 1$, which should be determined from the solution of the problem; nondimensionalizing is performed as follows: $\hat\rho$ and ρ are normalized by ρ_*; μ_0 and K_0 by μ_*; M by $(4/3)\pi\hat R_1^3\rho_*$ ($\rho_* = 1$ g/cm^3 and $\mu_* = 10^5$ MPa). To represent $\hat\rho$ and M as the functions of r', we interpolate the known values of these quantities at the nodes with the coordinates of the nodes $\hat r'$ using the dependence $r'(\hat r')$ available in the iteration. The boundary conditions $\hat\sigma_1 = P_1$ at $r' = 1$ and $\varepsilon_1 = \varepsilon_2$ at $r' = 0$ and the continuity condition for $\hat\sigma_1$ and ε_2 at the boundary points between the layers are satisfied.

The solution of system (4.8) satisfying the specified boundary conditions is found by the Runge–Kutta method as a solution of the problem with the initial conditions obtained at the point $r' = 1$ by specifying the value of the parameter ξ. For each ξ, formulas (4.6) and (4.7), we determine the values of J, ε_1, and $\varepsilon_2 = \varepsilon_{2(A)}$ for $r' = 1$ and the values of the constants α_1 and α. Runge–Kutta calculations are performed beginning from the point $r' = 1$ in the direction to the point $r' = 0$. In each layer, calculating ε_1 and, ε_2 and using the continuity condition for $\hat{\sigma}_1$ and ε_2 at the boundary point with the underlying layer, we obtain the values of ε_1 and ε_2 at this point for the underlying layer and then continue the calculations in this layer. To eliminate the uncertainty $0 : 0$ at the center $r' = 0$, the calculation in the inner core is performed only to the point $r'_\delta = 0.0005$. Iterations yield ξ that ensures calculation of ε_1 and ε_2 up to the point r'_δ at which the equality $\varepsilon_1 = \varepsilon_2$ is satisfied with sufficient accuracy. It should be noted that the value of ξ should be determined with high accuracy [15–18 digits after the comma to achieve smallness of the difference $(\varepsilon_1 - \varepsilon_2)$ of order 10^{-6} at the point r'_δ]. The errors of the solutions of Eqs. (4.8) (the values of the left sides of these equations) are represented by oscillating functions r' with reasonably small oscillation amplitudes, which are smaller in the central segments of the layers and increase when approaching the boundary points between the layers. For each layer B, C, D, E, and G, the integrals of the left sides of Eqs. (4.8) calculated from the variable point r' in the layer to the upper boundary of the layer have order not below than 10^{-6}.

Thus, the validity of the solutions of the equilibrium problems obtained using the outlined algorithm is confirmed by the fact that both Eqs. (4.8) and the integral equalities obtained from them by integrating over r' are satisfied with small errors.

We note that the numerical solution for the outer core obtained for the specified small shear modulus μ differs insignificantly from the analytical solution for $\mu = 0$ found by the formulas

$$p = \hat{\sigma}_1 = \hat{\sigma}_2 = (\hat{\sigma}_1 - P)_{\hat{r}=\hat{r}_D} + P, \qquad J = \Big(\frac{3K + 7p}{3K + 5p}\Big)^{3/2},$$

$$\varepsilon_2 = \hat{r}^2 \Big\{ \int\limits_{\hat{r}_D}^{\hat{r}} 3\hat{r}^2 J^{-1} d\hat{r} + \Big[(\hat{r}^{-2}\varepsilon_2)_{\hat{r}=\hat{r}_D}\Big]^{-3/2} \Big\}^{-2/3}, \qquad \varepsilon_1 = \Big(\frac{J}{\varepsilon_2}\Big)^2$$

using the values of P, $\hat{\sigma}_1$, and ε_2 are calculated in the mantle at the boundary to the outer core $\hat{r} = \hat{r}_D$. In the outer core, this solution corresponds to values of the density $\rho = J\hat{\rho}$, modulus $K_0 = 2K(7J^{-7/3} - 5J^{-5/3})^{-1}$, and radial coordinate $r' = \hat{r}'(\varepsilon_{2(A)}/\varepsilon_2)^{1/2}$, which are close to the data of Table 1.

Table 1 gives the density ρ, shear and bulk moduli μ_0 and K_0, and Poisson's ratio ν_0 for the unstrained material. Let us consider the distributions of these values on the segment $0 < \hat{r}' < 1$. The bulk modulus K_0 typically increases with depth. Characteristic features of K_0 are a small decrease in passing from the outer core to the inner core and the presence of a weak minimum in the outer core near the boundary to the mantle. The sharp increase in K_0 due to passage from the mantle to the outer core is much larger than that in K.

The distributions of μ_0, ν_0, and μ, ν are similar. In layers B and C, Poisson's ratio ν_0 takes maximum values in the limit when approaching the boundary point between these layers, at which ν_0 decreases sharply in passing from B to C; in most of layer D, the value of ν_0 changes insignificantly, increasing with approach to layer C and decreasing with approach to the outer core. In the outer core, Poisson's ratio ν_0 (as well as ν in the compressed state of the Earth) is close to 0.5. Over the entire range of the solution, $0 < \nu_0 < 0.5$.

The density of the material in the unloaded state ρ typically increases with depth. At the boundary between the mantle and the core, its sharp increases is somewhat greater than that of for $\hat{\rho}$. Characteristic features of ρ are weak minima in layer D, in the outer core, and at the center $\hat{r}' = 0$ and a small sudden decrease in passing from the outer core to the inner core.

In Figs. 1–5, the curves of the functions versus $\hat{r}'$ undergo discontinuities at the boundary points between layers B and C, between the mantle and the outer core, and between the outer core and the inner core. At these boundary points, the functions undergo a sudden change. The figures give the values of $\hat{\sigma}_1$, $\hat{\sigma}_2$, P, Ψ, Ψ_1, and Ψ_2 referred to μ_*.

Figure 1 shows curves of the stresses $\hat{\sigma}_1$ and $\hat{\sigma}_2 = \hat{\sigma}_3$ and purely hydrostatic compression pressure P versus $\hat{r}'$. The radial stress $\hat{\sigma}_1$ (solid curve) changes continuously and increases with depth. The circumferential stresses $\hat{\sigma}_2$ (dashed curve) increase with depth inside the layers; they increase suddenly in passing from layer B to layer C and decrease in passing from the mantle to the outer core and from the outer core to the inner core. In the mantle, $\hat{\sigma}_1$

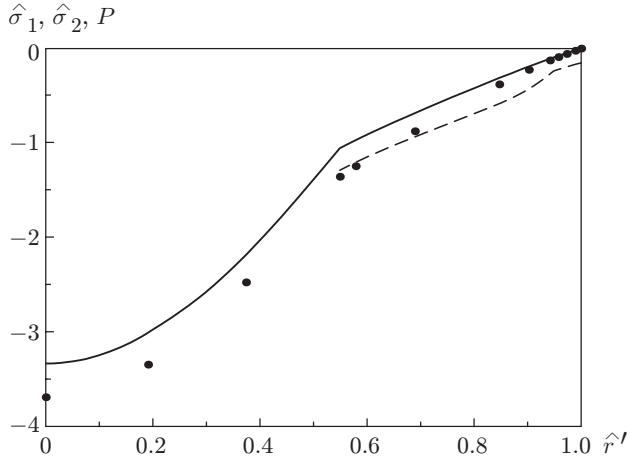

Fig. 1

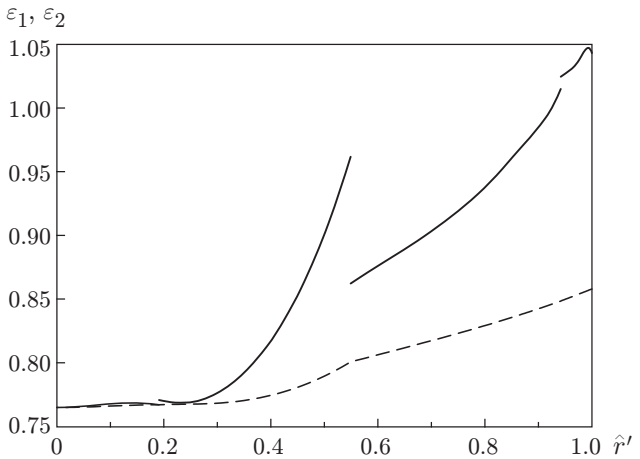

Fig. 2

and $\hat{\sigma}_2$ have significantly different values; on the boundary surface $\hat{r}' = 1$, the circumferential stresses are almost 19 times higher than the radial stresses. As the depth increases, the stress difference $(\hat{\sigma}_1 - \hat{\sigma}_2)$, decreasing somewhat in layer B, increases suddenly in passing to layer C and, continuing to increase, reaches the maximum in layer D, and then decreases in the mantle. In the mantle at the boundary to the outer core, $\hat{\sigma}_2$ is approximately 22% higher than $\hat{\sigma}_1$. In the stress state in the core, the stresses $\hat{\sigma}_1 \approx \hat{\sigma}_2 \approx p$ are almost identical. In the mantle, the purely hydrostatic compression pressure P (shown by points in Fig. 1) increases with depth and approaches the value of $\hat{\sigma}_2$. In the core, the stresses are lower than P; at the center, they are approximately 10% lower.

The variability of μ_0, K_0, and ρ is responsible for the complex distribution of the strains along the Earth's radius in the case of adiabatic or isothermal stress relief. In Fig. 2, the solid and dashed curves show the squares of the main multiplicities of the elongations ε_1 and ε_2 as functions of $\hat{r}'$. [In considering the strained state, one should bear in mind that in the radial and circumferential fibers $(i = 1, 2)$ in the case of tensile strain $\varepsilon_i > 1$, stress relief leads to shortening, and in the case of compressive strain $\varepsilon_i < 1$, it leads to elongation; in the case of bulk compressive strain $J < 1$, stress relief leads to an increase in the volume of the material, which is the larger the stronger the compression.] In the circumferential direction, we have compressive strain $\varepsilon_2 < 1$ (dashed curve); as the depth increases, ε_2 changes continuously and decreases. We note a considerable compressive strain of the circumferential fibres $\varepsilon_2 = 0.8579$ on the surface $\hat{r}' = 1$; at the center, $\varepsilon_1 = \varepsilon_2 \approx 0.7648$.

In the radial direction in the mantle to a depth of 506 km (reckoned from the surface $\hat{r} = \hat{R}$), we have tensile strain $\varepsilon_1 > 1$ (solid curve in Fig. 2), and in layer B, the value of ε_1 and elongation of the radial fibers increase with depth from $\varepsilon_1 = 1.0431$ at $\hat{r}' = 1$ to the maximum $\varepsilon_1 = 1.0473$ at a depth of 71.7 km, after which ε_1 in the mantle decreases. In passing from the mantle to the outer core, the value of ε_1 increases suddenly, the radial strain in the outer core is much smaller than the circumferential strain despite the nearly equal stresses $\hat{\sigma}_1 \approx \hat{\sigma}_2$. With depth, ε_1 decreases, approaching ε_2. There is a minimum of ε_1 at the boundary to the inner core. In passing to the inner core, ε_1 decreases sharply.

In the inner core, with closeness of the values of $\varepsilon_1 \approx \varepsilon_2$ there is a complex nature of variation in the value of ε_1, which practically coincides with ε_2 at the boundary to the outer core, increases with distance from the boundary to reach a maximum, and then decreases, approaching ε_2. The value of ε_2 in the inner core decreases monotonically.

Bulk compressive strain $J < 1$ occurs over the entire sphere (Fig. 3) but the compression is minimum not on the surface $\hat{r}' = 1$, where $J = 0.8762$, but at a depth of 56.8 km with $J = 0.8771$. Characteristic features of J are a sudden decrease in passing from layer B to layer C and from the outer core to the inner core and a sudden increase J in passing from the mantle to the outer core. There are a minimum of J in the outer core near the boundary to the inner core and a local maximum of J in the inner core. The maximum compression is reached at the center $\hat{r}' = 0$, where $J \approx 0.6689$.

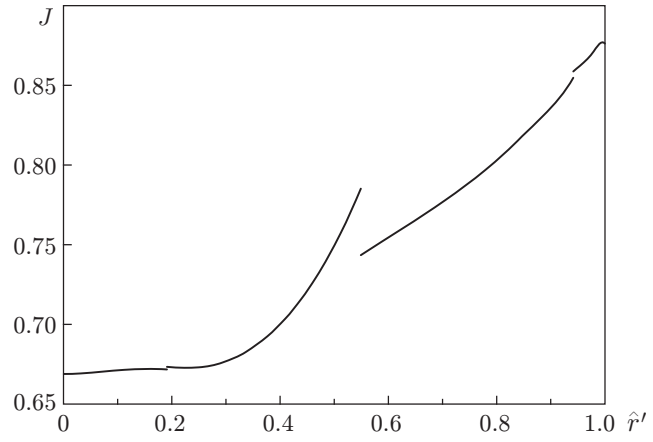

Fig. 3

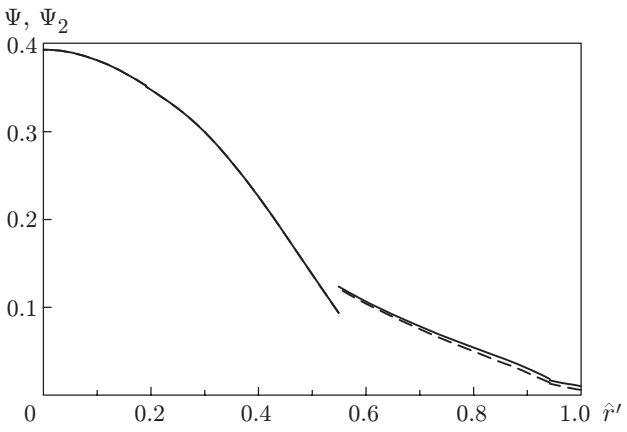

Fig. 4

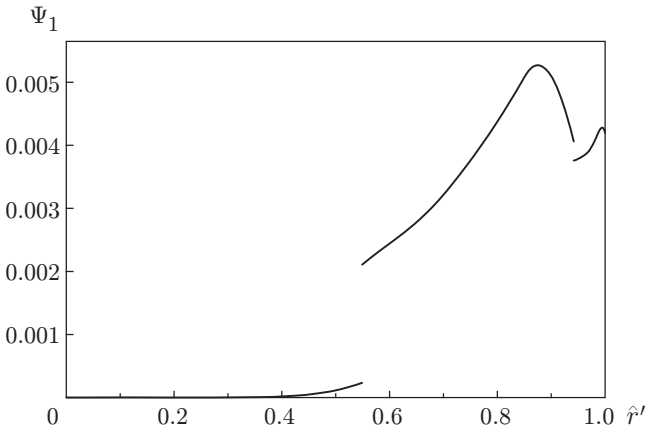

Fig. 5

The quantity Υ characterizes the shear strain intensity. In layer B, it increases with depth from $\Upsilon = 0.003004$ on the surface $\hat{r}' = 1$ to the maximum over the entire sphere $\Upsilon = 0.00318$ at a depth of 81.6 km, after which the value of Υ decreases in the mantle. The value of Υ decreases suddenly in passing from layer B to layer C and increases suddenly in passing from the mantle to the outer core. In the outer core, Υ decreases with depth, reaches a minimum near the boundary to the inner core, then increases somewhat, and decreases suddenly in passing to the inner core. In the inner core, Υ is negligible and has a local maximum here.

With increase in depth, the strain energy densities Ψ and Ψ_2 (shown by the solid and dashed curves in Fig. 4) increase everywhere, except at the point of passage from the mantle to the outer core, where they decrease suddenly. The shear strain energy density $\Psi_1 = \Psi - \Psi_2$ (Fig. 5) changes in a more complex manner. It has maxima: the smaller $\Psi_1 = 428$ MPa at a depth of 64.3 km and the larger $\Psi_1 = 527$ MPa at a depth of 821.8 km. A characteristic feature of Ψ_1 is a considerable sudden decrease with passage from the mantle to the outer core. On the boundary $\hat{r}' = 1$, the contribution of Ψ_1 to the value of Ψ is 41%, and with increase in depth in the mantle, it decreases. In the outer and inner cores, Ψ_1 and its contribution to Ψ are negligible.

Table 2 gives the values of r', $(r - \hat{r})$, ε_1, ε_2, J, $\hat{\sigma}_1$, $\hat{\sigma}_2$, p, P, Ψ_1, and Ψ_2 at the nodes; the values at the center are approximate values calculated at the close point $r' = 0.001$. The values of the differences $(r - \hat{r})$ are the increments in the nodal coordinates due to passage from the compressed to the unloaded condition. Thus, the radius of the boundary surface $\hat{R}_1 = 6341$ km increases to $R_1 = 6846$ km, i.e., by $R_1 - \hat{R}_1 = 505$ km.

TABLE 2

Stressed and Strained State

Node	r'	$r-\hat{r}$, km	ε_1	ε_2	J	$\hat{\sigma}_1$, 10^3 MPa	$\hat{\sigma}_2$, 10^3 MPa	P, 10^3 MPa	Ψ_1, 10^3 MPa	Ψ_2, 10^3 MPa
1	1	505	1.0431	0.8579	0.8762	−0.841	−15.94	−0.841	0.4197	0.6045
2	0.990	506.6	1.0461	0.8561	0.8756	−2.82	−17.67	−3.15	0.4229	0.7079
3	0,9757	508,6	1,0359	0,8535	0,8687	−5.69	−20.17	−6.494	0.3953	0.8955
4	0.9613	510.2	1.0292	0.851	0.8633	−8.61	−22.94	−9.887	0.382	1.098
5	0.9469	511.5	1.0245	0.8484	0.8577	−11.57	−25.85	−13.32	0.3758	1.311
	0.9469	511.5	1.015	0.8484	0.8547	−11.57	−27.84	−13.32	0.4061	1.429
6	0.9104	511.3	0.9859	0.8427	0.8367	−19.82	−43.46	−23.31	0.5062	2.502
7	0.8585	506.4	0.9594	0.8351	0.818	−31.9	−59.06	−38.69	0.5035	3.846
8	0.7068	467.5	0.9001	0.8161	0.7742	−69.11	−94.12	−88.22	0.3114	7.812
9	0.5981	423.4	0.8704	0.8039	0.75	−97.46	−121	−125.1	0.2309	11.11
10	0.5684	409.3	0.8621	0.8007	0.7434	−106.1	−129.4	−136.3	0.2107	12.16
	0.5684	409.3	0.9617	0.8007	0.7852	−106.1	−107.1	−136.3	$2.324 \cdot 10^{-2}$	9.363
11	0.3942	327.5	0.8028	0.772	0.6917	−218.7	−218.9	−247.9	$8.9 \cdot 10^{-4}$	24.73
12	0.202	171.8	0.7707	0.767	0.6733	−300.1	−300.2	−334.8	$1.3 \cdot 10^{-5}$	35.13
	0.202	171.8	0.767	0.767	0.6717	−300.1	−300.1	−334.8	$1.4 \cdot 10^{-9}$	35.23
13	0	0	0.7648	0.7648	0.6689	−333.5	−333.5	−369.1	0	39.35

Conclusions. 1. Distributions of the shear and bulk moduli μ_0 and K_0 in adiabatic or isothermal processes of stress relief and the material density ρ in the unstrained state were obtained.

2. The theory of isotropic hyperelastic bodies suggests that in the mantle there is anisotropy of the material resistance to additional deformation, which influences the propagation of body waves generated by seismic disturbances.

3. The stress state in the mantle differs considerably from the state of purely hydrostatic compression. The circumferential stresses at the upper boundary of the region far exceed the radial stress, resulting in a strong compression of circumferential fibers at this boundary. At the center of the Earth, the pressure is approximately 10% lower than the purely hydrostatic compression pressure.

4. In the mantle to a depth of 506 km, radial tensile strains rather than compressive strains occur, which reach a maximum at a depth of 71.7 km. In the outer core near the boundary to the mantle, the radial and circumferential strains differ considerably (although $\hat{\sigma}_1 \approx \hat{\sigma}_2$).

5. Bulk compressive strain occurs over the entire region ($J < 1$), but with increase in depth starting from the boundary surface, the compression decreases rather than increases, reaches a minimum at a depth of 56.8 km, and then increases in the mantle. The maximum bulk compressive strain occurs at the center of the Earth.

6. The shear strain energy density Ψ_1 makes a considerable contribution to the total strain energy density Ψ near the boundary surface. As the depth increases, the contribution of Ψ_1 decreases rapidly and becomes negligible in the core. The maxima of Ψ_1 are reached at depths of 64.3 km (the smaller maximum) and 821.8 km (the larger maximum).

7. The employed algorithm provides a high-accuracy solution of the equilibrium problem, which is confirmed by the fact that the conditions of the problem are satisfied with small errors.

This work was performed within the framework of integration project of the Siberian Division of the Russian Academy of Sciences (Project No. 82) and supported by the Russian Foundation for Basic Research (Grant No. 02-01-00195).

REFERENCES

1. K. E Bullen, *The Earth Density*, Wiley, New York (1975).
2. Sir H. Jeffreys, *The Earth*, Cambridge Univ. Press, Cambridge (1970).
3. A. M. Dziewonsky and F. Gilbert, "Observations of normal modes from 84 recordings of the Alaskan earthquakes of 1964 March 28, II. Further remarks based on new spheroidal overtone data," *Geophys. J. Astr. Soc.*, **35**, 401–437 (1973).
4. T. N. Jordan and D. L. Anderson, "Earth structure from free oscillations and travel times," *Geophys. J. Astr. Soc.*, **36**, 411–459 (1974).
5. V. N. Solodovnikov, "Constitutive equations of an isotropic hyperelastic body," *J. Appl. Mech. Tech. Phys.*, **41**, No. 6, 1118–1123 (2000).
6. V. N. Solodovnikov, "Stability of deformation of isotropic hyperelastic bodies," *J. Appl. Mech. Tech. Phys.*, **42**, No. 6, 1043–1052 (2001).
7. V. N. Solodovnikov, "On the theory of deformation of isotropic hyperelastic bodies," *J. Appl. Mech. Tech. Phys.*, **45**, No. 1, 99–106 (2004).
8. F. Birch, "Elasticity and constitution of the Earth's interior," *Geophys. Res.*, **57**, 227–286 (1952).
9. F. D. Murnaghan, *Finite Deformation of Unelastic Solid*, John Wiley and Sons, New York (1951).